PIER C

(Received 17 February 2025, Accepted 14 April 2025, Scheduled 22 April 2025)

Ternary B_2O_3-TeO_2-BaO Glass as a Shielding Case

Samar M. Ibrahim*, Yara Abdelghany, Maged M. Kassab, Mostafa M. Radwan, and Ahmed Abdel-Latif M

Department of Mathematics and Engineering Physics, Faculty of Engineering, Fayoum University, 63511 Fayoum, Egypt

ABSTRACT: This study investigates the properties of a ternary B_2O_3-TeO_2-BaO glass system, prepared through the melt-quenched technique. The chemical formula used is $\left(50-\frac{x}{2}\right)B_2O_3+\left(50-\frac{x}{2}\right)TeO_2+x$BaO, with x varying from 15 to 35 mol.%. The research explores how the gamma and neutron radiation shielding capabilities were analyzed. It finds that higher BaO content enhances gamma-ray shielding but does not significantly affect neutron shielding. The glass sample BTB35 emerged as the optimized candidate among the developed samples for gamma radiation shielding applications. Also, the obtained results for the MFP was compared to commercial shielding glasses, and other measurements on glasses show the superiority of BTB35 as commercial transparent radiation shielding glass.

1. INTRODUCTION

Nuclear energy is important for global economic growth and energy sustainability. Alongside renewable energy, it offers a significant opportunity for reducing carbon emissions due to its low-carbon nature [1–3]. However, The production of nuclear energy generates nuclear radiation, which can harm living beings by causing skin burns, reducing white blood cell counts, and increasing cancer risk [4–7]. Proper shielding materials, often made of lead, can effectively reduce radiation exposure and risks; however, the search for safer alternative materials is ongoing due to the hazards associated with lead in nature [8]. Concrete is a widespread material used for radiation shielding in nuclear power plants because of its low permeability, fire resistance, and ability to be molded [9, 10]. Radiation shielding concrete (RSC) specifically is a heavyweight concrete used in facilities for creating protection domes and storing spent nuclear fuel [11–13]. Research has focused on enhancing its shielding effectiveness through compositional changes while maintaining modest thickness [14, 15]. Concrete, despite being an effective radiation barrier, has drawbacks, including losing water content due to long-term exposure leading to internal tensile stress and fractures, as well as being heavy, expensive, and opaque. This has led scientists to investigate alternative materials [16]. Glass materials, compared to concrete and lead, have numerous advantages such as transparency, economic efficiency, lightweight properties, ease of production, and non-toxicity. They serve as promising alternatives for radiation shielding as a result of their favorable chemical, physical, and structural properties, particularly their effectiveness in attenuating electron and gamma-ray radiation [17]. Boric acid (B_2O_3) is recognized as an excellent glass former that can be combined with other materials like tellurite (TeO_2) to create boro-tellurite glasses [18, 19]. These glasses possess distinctive optical and shielding properties, making them ideal for photonic applications. They can also be doped with rare-earth elements to enhance their luminescence [20, 21]. The incorporation of tellurium enhances their shielding capabilities against gamma and X-rays, benefiting various radiation-sensitive environments, such as medical imaging and nuclear facilities [22]. Studies have demonstrated that adding barium oxide (BaO) to boro-tellurite glass systems greatly enhances their structural, physical, and radiation-shielding properties. BaO increases both refractive index and density, improves flexibility, and increases the effectiveness of radiation shielding through changing the glass network. These characteristics make these glasses especially appropriate for applications involving high-performance optical devices [23]. However, prior formulations often struggled with efficiency against specific radiation types and faced issues related to density, optical clarity, cost, and environmental impact [24, 25].

This research aims to explore the outcome of BaO on the radiation shielding capabilities of a novel barium boro-tellurite that presents a glass composition designed to address these challenges. Five glass samples were fabricated with the composition $\left(50-\frac{x}{2}\right)B_2O_3+\left(50-\frac{x}{2}\right)TeO_2+x$BaO varying BaO content ($x=15$, 20, 25, 30, and 35 mol.%). These samples underwent X-ray diffraction (XRD) analysis, and their radiation shielding specifications were assessed theoretically.

2. MATERIAL AND METHODS

This section outlines the methods for glass preparation and the formulas used to assess its radiation shielding characteristics.

2.1. The Fabrication of Glass Samples

Five glass test pieces were fabricated via the classic melt-quenching approach as shown in Figure 1, labeled BTB15, BTB20, BTB25, BTB30, and BTB35, with varying compositions (where $x=$ 15, 20, 25, 30, and 35 mol.%). The batch was made with premium raw materials and analytical reagents including H_3BO_2 (61.83 g/mol), TeO_2 (159.58 g/mol),

* Corresponding author: Samar M. Ibrahim (sma33@fayoum.edu.eg).

FIGURE 1. Glass manufacture by *melt-qunching technique procedure.*

TABLE 1. The mass content of each raw material in 15 gram glass samples based on Matlab code.

Glass Sample	BTB15	BTB20	BTB25	BTB30	BTB35
$BaO(OH)_2.8H_2O$ mass (g)	3.11	4.06	4.96	5.83	6.66
TeO_2 mass (g)	4.28	3.94	3.62	3.31	3.00
H_3BO_2 mass (g)	7.61	7.00	6.42	5.85	5.34

and $BaO(OH)_2.8H_2O$. Every chemical, with purities exceeding 99.9%, was obtained from DOP Company. MATLAB software [26] was used to determine the glass batch composition, which is shown in Table 1. Weighting, grinding, and properly combining 15 grams of these raw materials took about 15 minutes, using a pestle and mortar for blending in a porcelain crucible. After the materials were preheated to approximately 650°C, they were heated in (Magma Thermal high-temperature electric furnace), where the temperature was amplified at 5°C/min. Melting at 900°C is for 60 minutes until the melt became homogeneous, clear, and free of bubbles. Once the melt was uniform, the molten glass was quickly cooled by pouring it into a rectangle copper mold sized ($1 \times 0.5 \times 0.3$ cm) and subsequently quenching it with a plate. As a result, the glass samples became optically translucent. After three hours of annealing at 450°C in a muffle furnace, the glass samples were permitted to reach ambient temperature for around 24 hours in order to release internal stresses.

2.2. XRD Investigation

X-ray diffraction was employed to evaluate the produced samples' glassy qualities. The tests employed Ni-filtered Kα-Cu radiation $\lambda = 1.541$Å and were conducted across a 2θ range of (5–60 degrees), with a scanning rate 8 degrees/minute.

2.3. Radiation Shielding Characteristics: Theoretical Background

The effectiveness of materials' shielding is assessed using simulation method, enabling material composition adjustments before manufacture. Shielding parameters including effective fast neutrons removal cross-section, mass attenuation coefficient, and linear attenuation coefficient are estimated by using PHY-x/PSD [27] and NGCAL [28] codes.

Density is an important physical parameter that must be calculated to investigate radiation shielding characteristics. The following equation was applied to compute the theoretical density of the produced glass specimens [29].

$$\rho = \frac{100}{\sum_{i=1}^{3} \frac{w_i}{\rho_i}} \tag{1}$$

where ρ_i denotes the density, and w_i denotes the weight percentage of the i^{th} oxide of the glass composition.

The radiation shielding characteristics of the fabricated glass were investigated and theoretically assessed using Phy-X/PSD software over a continuous energy of photon spectrum of 0.01–15 MeV. The following Lambert-Beer's formula allows for the calculation of the linear attenuation coefficient [30, 31].

$$\mu = \ln\left(\frac{I}{I_0}\right)/d \tag{2}$$

where I denotes the intensity of transmitted photons, and I_0 denotes the intensity of incoming photon, whilst d is the glass' thickness. The mass attenuation coefficient for any combination of materials may be computed using the formula below [32]:

$$\mu_m = \sum_i w_i \left(\frac{\mu}{\rho}\right)_i = \sum_i w_i \left(\mu_m\right)_i \tag{3}$$

The weight fraction denoted by w_i and mass attenuation denoted by $(\mu_m)_i$ of the i$^{\text{th}}$ ingredient. Radiation Protection Efficiency (RPE) measures how effectively a material or shield minimizes radiation exposure. It is usually expressed as a percentage, calculated by [33]:

$$\text{RPE} = \frac{I_o - I}{I_o} * 100 = 100 * (1 - \exp(\mu d)) \tag{4}$$

This parameter gives a clear indication of the material's ability to protect against radiation. A higher RPE indicates more effective radiation shielding.

A key parameter for shielding is the mean free path (MFP) which serves as the equivalent of the linear attenuation coefficient. It describes how gamma rays interact with the glass system and reflects the shielding efficiency of a material [34].

$$\text{MFP} = \frac{1}{\mu} \tag{5}$$

A key concept to define photon interactions with matter is effective atomic number (Z_{eff}). However, for composite materials the way that a material interacts with photons is unable to

be accurately represented by a single atomic number. Instead, it may be determined using Equation (6) provided below [35, 36]. Z_{eff} is reliant on the chemical structure and photon energy of the interacting glasses. A single value is unable to accurately represent the atomic number in each of the several energy zones. So-called "effective atomic number" (Z_{eff}) fluctuates with photon energy and is used to describe compounds or composite materials. It shows the corresponding atomic number of atoms in a chemical combination or mixture that interact similarly with photons [37]. The effective atomic number (Z_{eff}) is an indicator utilized to evaluate the productivity of a shielding substance that contains many elements. A glass system with a greater Z_{eff} value thus appears t more efficient at attenuating the incoming photons than the one with a smaller Z_{eff} value. A larger value of Z_{eff} indicates that the material has more capacity to block the incidence radiation [38].

$$Z_{eff} = \frac{\sum_i f_i A_i \left(\frac{\mu}{\rho}\right)_i}{\sum_i \frac{f_i A_i}{Z_i} \left(\frac{\mu}{\rho}\right)_i} \tag{6}$$

where $(\mu/\rho)_i$, A_i, Z_i, and f_i represent the mass attenuation coefficient, atomic weight, the atomic number, and the number of atoms of the i^{th} ingredient oxide relative to the total number of atoms in the composition, respectively.

Fast neutrons, with energies over 1 MeV, pose significant radiation risks due to their high kinetic energy and indirect ionization. Shielding fast neutrons is difficult since they are neutral and do not lose energy through direct ionization like charged particles or gamma rays. The likelihood that a fast neutron will slow down to thermal energy and be eliminated from the fast neutron flux is indicated by a material's effective removal cross-section ($\sum R$). This measurement helps estimate a material's ability to moderate neutrons and assists in designing shielding configurations [39]. An approximate method exists for computing fast neutron attenuation using $\sum R$, though not all interactions lead to removal, affecting its reliability [40, 41]. The effective removal cross-section is slightly changing, between 4 and 12 MeV, making it useful in various experimental scenarios [42]. For compounds and homogeneous mixtures, a particular equation below may be utilized to deduce macroscopic effective removal cross-sections, also known as linear neutron attenuation coefficients (ΣR) [43]:

$$\sum R = \sum_i \rho_i \left(\frac{\sum R}{\rho}\right)_i = \sum_i \omega_i \rho \left(\frac{\sum R}{\rho}\right)_i \tag{7}$$

In this context, ρ and $\left(\frac{\sum R}{\rho}\right)_i$ denote the weight fraction and density, while ω_i is the weight percentage and i^{th} the mass removal cross-section of each component, correspondingly. The following expression can be applied to evaluate the mass neutron attenuation coefficient $\left(\frac{\sum R}{\rho}\right)$ for a given element [40]:

$$\left(\frac{\sum R}{\rho}\right) = 0.125 Z^{-0.565} for Z > 8 \tag{8}$$

$$\left(\frac{\sum R}{\rho}\right) = 0.19 Z^{-0.743} for Z \leq 8 \tag{9}$$

It is important to point out that lighter elements have a greater impact on the overall removal cross-section than heavier components. Therefore, as the weight fraction of light elements rises, their contribution to the effective removal cross-section also rises, and the opposite is true for heavier elements. The NGCAL algorithm [28] was implemented to assess the effective removal cross-section at 0.025 MeV for thermal neutrons and at 4 MeV for fast neutrons. In addition, the Phy-X/PSD algorithm [27] was utilized to evaluate the effective removal cross-section for fast neutrons ranging from 1.0 MeV to 4.0 MeV. For fast neutrons with very high energies (E), we applied Equations (7) to (9) in our calculations.

3. RESULTS AND DISCUSSION

The following section will present the results and their corresponding interpretations.

3.1. X-Ray Diffraction Spectra

Figure 2 depicts patterns of (XRD) X-ray diffraction of Barium boro-tellurite glass with different contents of barium oxide. This figure affirms the amorphous (glassy) type of the glass, as revealed by the lack of sharp peaks that would indicate a crystalline structure. The absence of crystalline peaks suggests that all of the barium oxide has been fully incorporated into the glass matrix. Each glass sample displays two humps. The wide halos are visible between 25° and 30°. Additionally, all samples exhibit a very faint second halo in the range of 41° to 48°, indicating that the glass is only marginally phase-separated. Subtle features like slight undulations or moderate broadening may indicate residual stress or the onset of microcrystallinity, but these interpretations should be made cautiously and supported by further research.

3.2. Gamma-Ray Radiation Shielding Characteristics

The density variation (ρ) with raising of BaO content is illustrated in Figure 3. As the concentration of BaO increases, the levels of B_2O_3 and TeO_2 oxides decrease, resulting in a density rise from 4 4.299 to 4.620 g/cm^3. Replacing B_2O_3 (Density: 2.46 g/cm^3, MW: 69.62 g/mol) with BaO (Density: 5.72 g/cm^3, MW: 153.33 g/mol) increased the glasses' density [44].

The fundamental shielding characteristics were obtained by Phy-X/PSD algorithm, which covers the photon energy spectrum from 0.015 to 15 MeV. These characteristics are the effective atomic number (Z_{eff}), linear attenuation coefficient (LAC), mean free path (MFP), and mass attenuation coefficient (μ_m). The linear attenuation coefficient (LAC) values for the $\left(50 - \frac{x}{2}\right) B_2O_3 + \left(50 - \frac{x}{2}\right) TeO_2 + xBaO$ glass system, where $x = 15$, 20, 25, 30, and 35 mol.%, are plotted against the incoming photon energy in Figure 4(a). The changes of linear attenuation coefficient values of all glass compositions follow a similar pattern increasing the incoming photon energy, and the linear attenuation values show an exponential decrease. It is clear that all samples' linear attenuation values are clearly at their maximum at low energy 0.015 MeV. Figure 4(b) illustrates the deviation of the linear attenuation coefficient μ over energy band from 0.015 to 0.08 MeV, where the photoelectric ef-

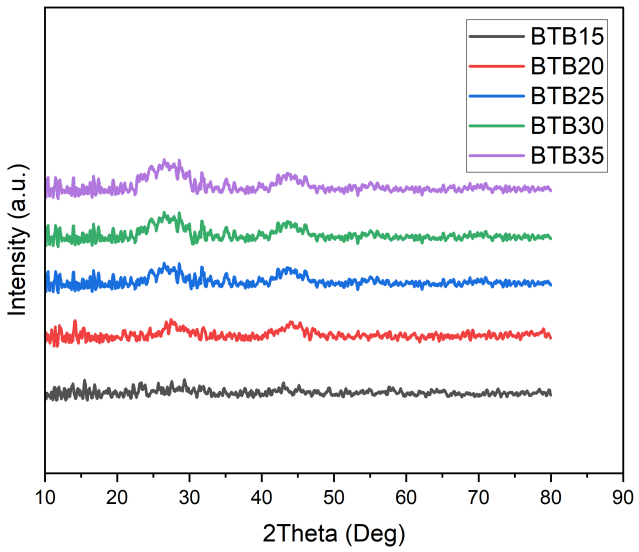

FIGURE 2. The fabricated glass samples' XRD patterns.

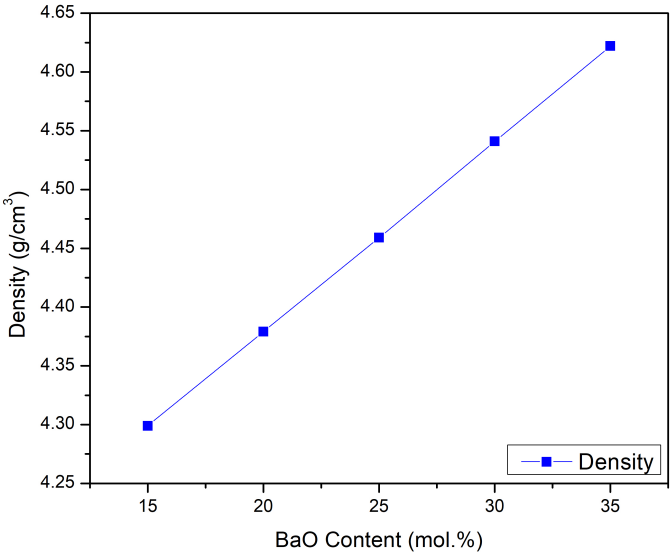

FIGURE 3. The glass density as a function of BaO concentration (%).

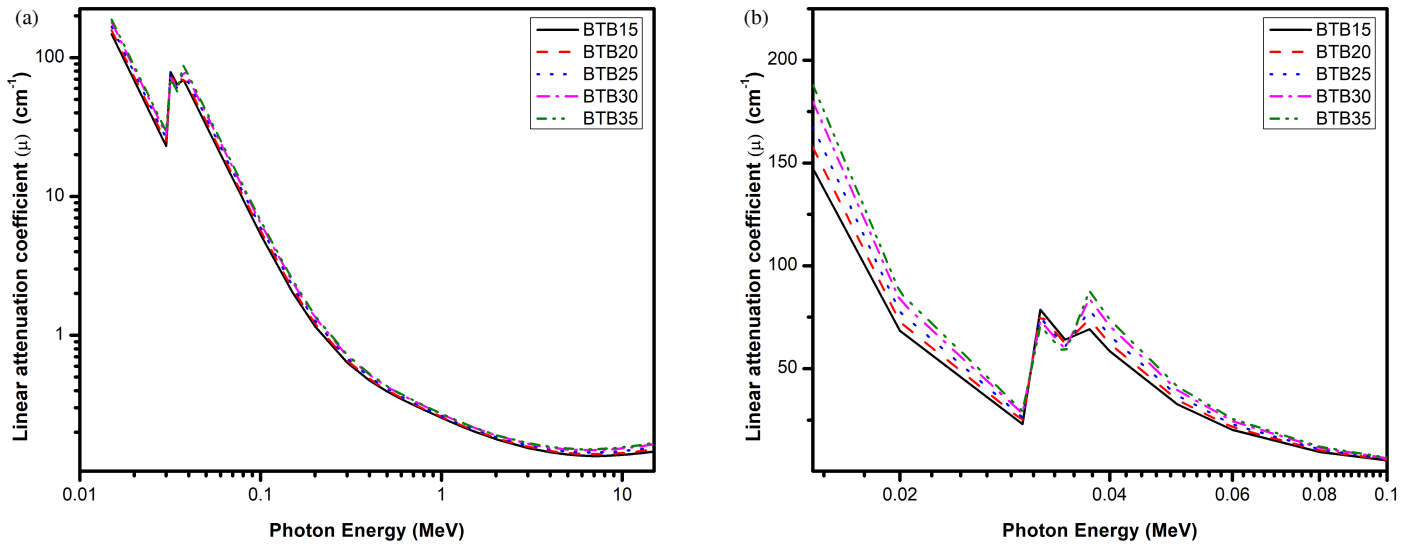

FIGURE 4. Relation between the linear attenuation coefficient for the synthesized glass (a) over the energy of photon band (15 KeV–15 MeV) (b) over the photon energy band (15 KeV–100 KeV).

fect is predominant, and μ decreases linearly with raising photon energy. Linear attenuation μ exhibits sharp peaks in energies 0.032 and 0.04 MeV. The presence of these two peaks are probably linked to the K-edge absorption energies of Te (0.0318 MeV) and Ba (0.0374 MeV), respectively. Figure 4(b) clearly shows that the K-absorption edge peak of Te appears obviously in the BTB15 sample, while the k-absorption edge peak of Ba appears obviously as the content of BaO rises.

For every glass sample investigated, the mass attenuation coefficient exhibits a consistent pattern as shown in Figure 5, and as the energy increases, the mass attenuation coefficient (MAC) values show an exponential decrease. This suggests that when being exposed to low energy radiation, the BTBX-glass composites function as effective shields. However, the photons' ability to attenuate grows weaker as energy rises.

Figure 6 depicts the impact of changing the BaO content (%) on the mean free path (MFP) at various energy lines. As demonstrated, the MFP increases with increasing energy but decreases with increasing BaO content. It can be shown that the BTB35 glass sample has the minimum values of MFP. Glass substances' capability to withstand radiation from gamma ions may also be explained through the MFP. A glass barrier that has the best protective capabilities is one with a smaller MFP value. In this context, it is evident that sample BTB35 has superior shielding properties.

The computed Z_{eff} values vs. energy of photon for $\left(50-\frac{x}{2}\right)B_2O_3 + \left(50-\frac{x}{2}\right)TeO_2$+xBaO glass system have been graphed in Figure 7. According to the findings, all glass samples show peak magnitudes at low energy (approximately 0.04 MeV). The comparable patterns in the μ and Z_{eff} spectra

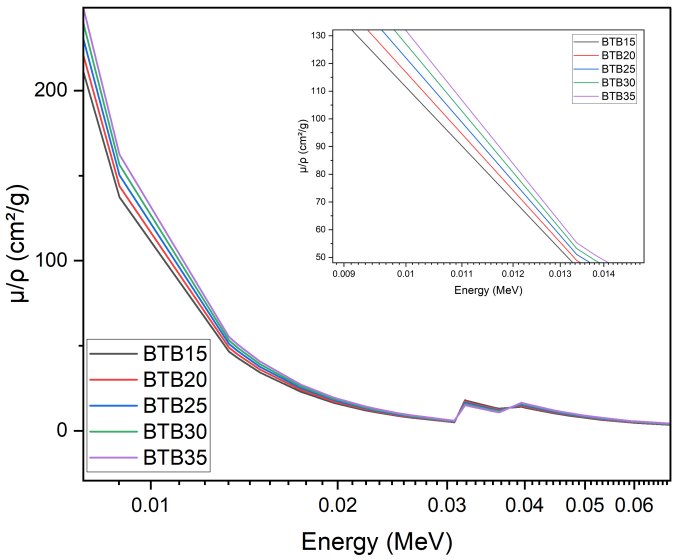

FIGURE 5. Mass attenuation coefficient for TeO_2-B_2O_3-BaO glass.

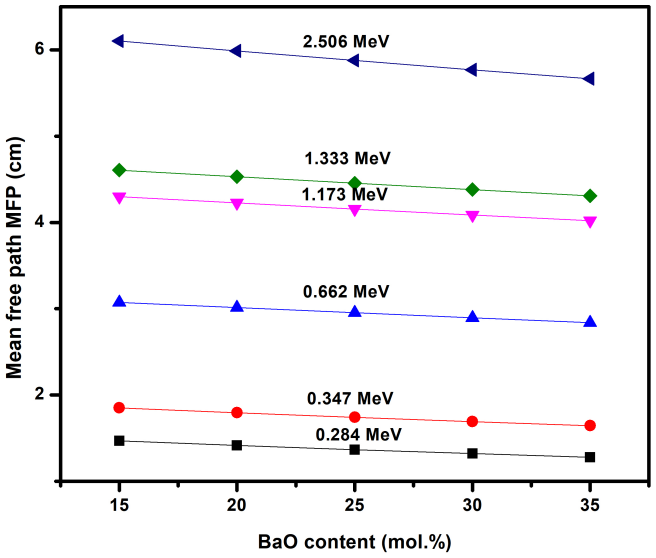

FIGURE 6. Variation of the mean free path (MFP) with BaO content over various energies.

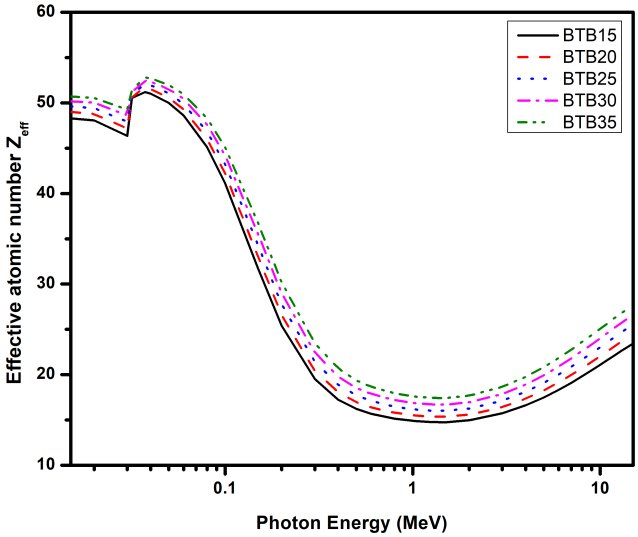

FIGURE 7. The relationship between the photon's energy and effective atomic number (Z_{eff}) for each sample.

suggest that the relative value of Z_{eff} could serve as a valuable indicator of the glasses' ability to shield against photons. The Z_{eff} values of the fabricated glass samples seem to rise when B_2O_3, and TeO_2 are replaced with BaO, while they decline as the photon energy increases. This demonstrated that materials with higher Z_{eff} values have a greater weight proportion of high Barium atomic number. The higher weight percentage of BaO and the ensuing high density appear to be the reason of BTB35's high effective atomic number.

Finally, Figure 8 represents how the BaO concentration affects the radiation protection effectiveness (RPE). In Figure 8(a), it is shown that the RPE of our glass samples sharply declines with increasing incident radiation energy, suggesting that they are best suited to defend against low-energy radiation. Overall, RPE curves flatten and decline slowly as the incoming

TABLE 2. Comparison of mean free path of the prepared glass samples vs. commercial and conventional concrete and glass at 662 keV.

Material classification	MFP (cm)	Reference
BTB35	2.839	This work
Ordinary concrete	5.5957	[26]
Hematite-serpentine concrete(Schott)	5.2219	[45]
Ilmenite-Limonite Concrete	4.6038	[46]
Basalt-Magnetite Concrete	4.2971	[47]
Ilmenite Concrete	3.8248	[47]
Steel-Scrap Concrete	3.3467	[48]
Steel-Magnetite Concrete	2.6481	[45]
RS 253 glass (Schott)	5.263	[49]
RS 253 G18 glass (Schott)	5.263	[49]
RS 323 G19 Glass (Schott)	3.571	[49]
RS 360 Glass (Schott)	3.125	[49]

radiation energy passes approximately 4 MeV, suggesting that shielding gets less sensitive to additional energy increases. In Figure 8(b), it is shown that radiation protection efficiency increases with increasing the content of BaO. Again, it is obvious that sample BTB35 has the highest value of RPE out of all the fabricated glass samples, which contains 35 mol.% BaO and is the most efficient gamma ray absorber.

Table 2 and Figure 9 present the mean free path (MFP) magnitudes at 0.662 MeV to evaluate the radiation efficiency of BTB35 in relation to other conventional shielding materials. When BTB35, the best attenuator among the glass samples under study was compared to regular concrete, RS 323 G19 Glass (Schott), hematite-serpentine concrete (Schott), ilmenite-limonite concrete, basalt-magnetite concrete, ilmenite concrete, steel-magnetite concrete, RS 253 glass (Schott), steel-scrap concrete, RS 253 G18 glass (Schott), and RS 360 glass (Schott), and the MFP was found to be the lowest. This suggests that

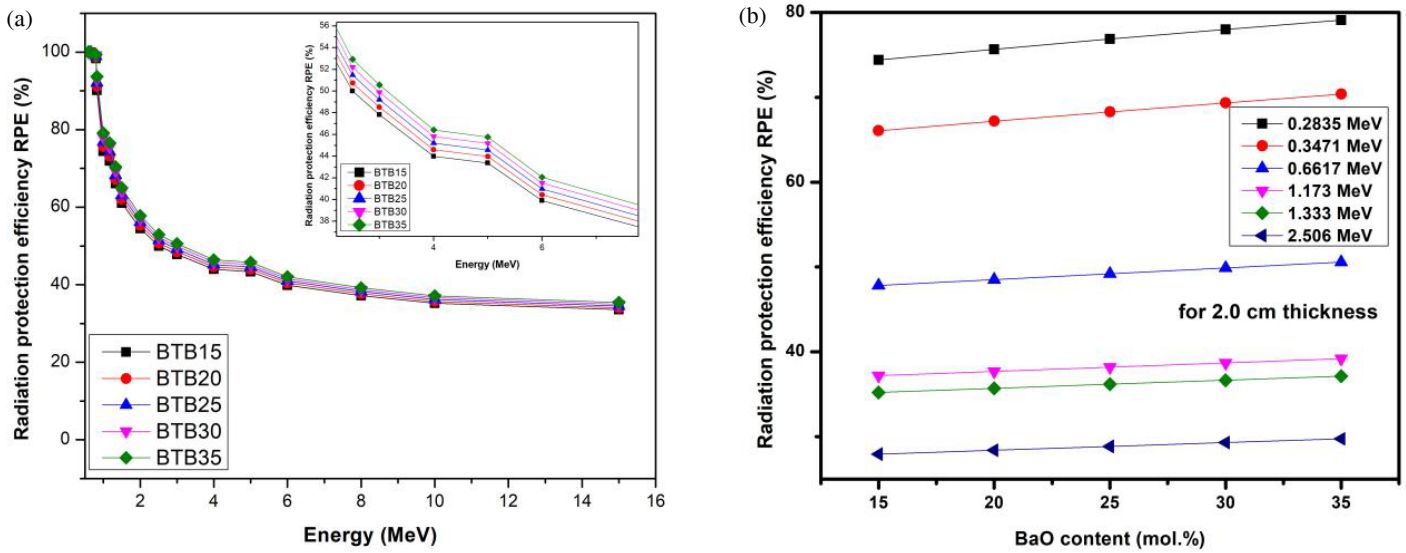

FIGURE 8. Variation of the Radiation Protection Efficiency (RPE) with Ba content (a) at energy range (0.01–15 MeV) and (b) at various energy lines.

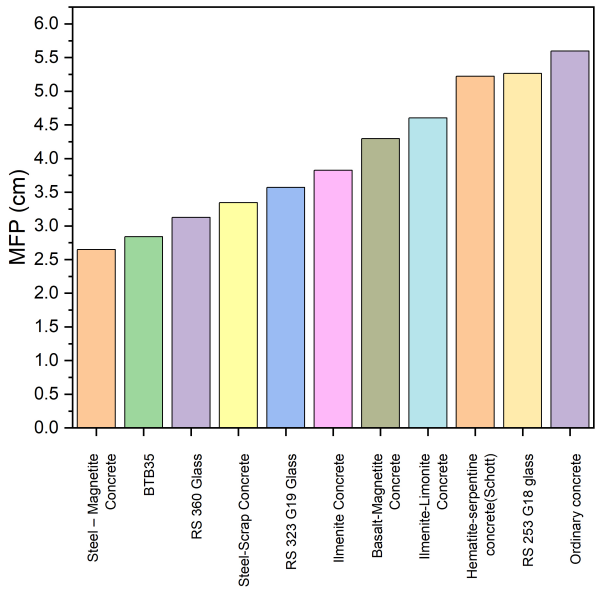

FIGURE 9. MFP comparison of the investigated glass vs. other types of shielding materials.

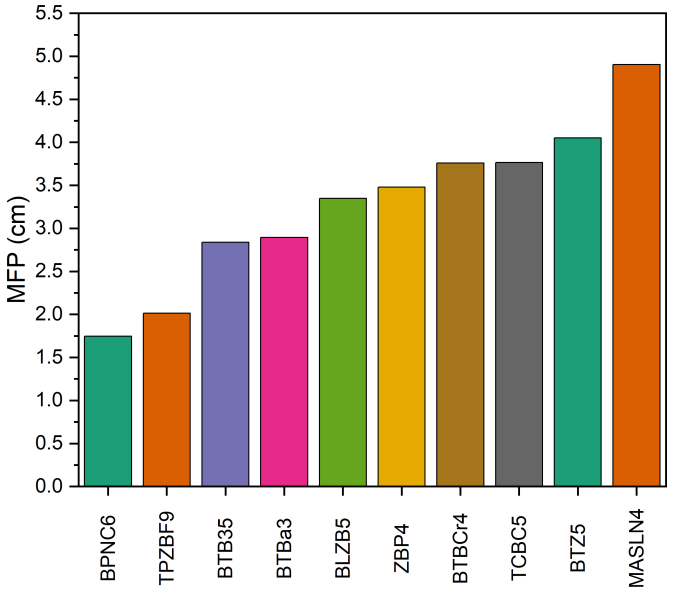

FIGURE 10. MFP comparison of the investigated glass vs. other types of shielding materials.

compared to other materials used in nuclear engineering, the glass under consideration, with the highest concentration of BaO, is a better choice for radiation shielding. Steel-Magnetite Concrete is still superior to our sample, nevertheless.

Also, the gamma radiation shielding effectiveness of the BTB35 sample has been contrasted with various previous glass shields based on their MFPs, which are graphed in Figure 10 and shown in Table 3. The comparison involved photons source energy is 662 keV. The figure indicates that BTB35 outperforms several other glass shielding materials, including BTBCr-4, BTZ5, MASLN4, ZBP4, TPZBF-9, TCBC5, BPNC6, and BTBa3. Notably, the MFP of BTB35 is significantly less than that of all the other selected glass samples, except for the unsafe lead-based glasses (BPNC6 and TPZBF-9). Additionally, its MFP is nearly identical to that of the BTBa3 glass.

To ensure safety in nuclear and medical applications, it is crucial to understand how fast neutrons are attenuated. This study investigates fast neutron attenuation by determining the effective thermal/fast neutron removal cross-section. Figure 11 summarizes the thermal neutron (0.0254 eV) and fast neutron (4.0 MeV) removal cross-sections calculated using the NGCAL code [28], as well as the effective fast neutron (1.0 MeV $< E <$ 4.0 MeV) removal cross-sections determined using the phys-X/PSD code [27] for various BaO contents. The observed drop in neutron attenuation that occurs when the amount of BaO in boro-tellurite glass increases is probably caused by the displacement of other elements that are better at attenuating neutrons, such as boron. Neutron interaction possibilities for the relevant energy range may also not be improved by small variations in the density and composition of the glass. In contrast to

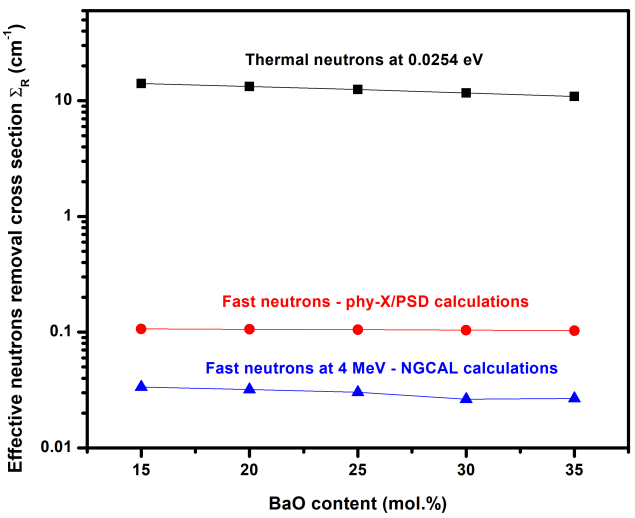

FIGURE 11. Variation of the removal cross-section of thermal neutrons, fast neutrons, and fast neutrons with the BaO content.

specific shielding substances, barium and oxygen are not very effective neutron attenuator. A prior report [24] has revealed a comparable outcome.

4. CONCLUSION

Five glass samples with varying BaO content (x = 15, 20, 25, 30, and 35 mol.%) were synthesized using the classic melt-quench approach. This research analyzed the radiation-shielding capabilities of the glasses. The findings are summarized as follows. The X-ray diffraction data exhibited a typical amorphous diffraction pattern with broad, diffuse haloes, confirming the glassy nature of the synthesized materials. The results indicate that increasing BaO content increases the density which enhances the effectiveness of gamma-ray radiation shielding. However, increasing the BaO content did not improve the removal cross-section for fast neutrons, indicating a limitation in neutron shielding efficiency. Notably, the glass sample BTB35 demonstrated superior performance in γ-radiation shielding applications. It was confirmed by comparing BTB35 results with other commercial materials. The greatest concentration BTB35 had the lowest mean free path, and higher mass attenuation coefficient. This glass sample yields results that are even superior to those of commercial radiation shielding glasses and regular concrete. It suggests that this glass has superior shielding properties and is more effective in attenuating the 662 keV gamma ray.

The practical use of BTB35 glass, while offering excellent gamma radiation shielding enhanced by BaO and transparency feature for areas like radio-pharmacy and hot labs, necessitates a balanced assessment of its drawbacks. The high cost due to expensive raw materials and the ongoing study of long-term environmental consequences must be weighed against its shielding benefits and transparency. A comprehensive evaluation of durability, cost-effectiveness, and environmental impact is essential to determine its appropriate applications.

TABLE 3. Prepared glasses' mean free path and other previous glass publications at 662 keV.

Type of material	MFP (cm)	Reference
BTB35	2.839	This work
BTBCr-4	3.758	[50]
BTZ5	4.05	[26]
MASLN4	4.905	[51]
ZBP4	3.479	[52]
TPZBF-9	2.012	[25]
BLZB5	3.3467	[53]
TCBC5	3.765	[54]
BPNC6	1.747	[44]
BTBa3	2.893	[49]

REFERENCES

[1] Albino, V., L. Ardito, R. M. Dangelico, and A. M. Petruzzelli, "Understanding the development trends of low-carbon energy technologies: A patent analysis," *Applied Energy*, Vol. 135, 836–854, 2014.

[2] Hong, S., C. J. A. Bradshaw, and B. W. Brook, "Global zero-carbon energy pathways using viable mixes of nuclear and renewables," *Applied Energy*, Vol. 143, 451–459, 2015.

[3] Prăvălie, R. and G. Bandoc, "Nuclear energy: Between global electricity demand, worldwide decarbonisation imperativeness, and planetary environmental implications," *Journal of Environmental Management*, Vol. 209, 81–92, 2018.

[4] Heffron, R. J., S. F. Ashley, and W. J. Nuttall, "The global nuclear liability regime post Fukushima Daiichi," *Progress in Nuclear Energy*, Vol. 90, 1–10, 2016.

[5] Lovering, J. R., A. Yip, and T. Nordhaus, "Historical construction costs of global nuclear power reactors," *Energy Policy*, Vol. 91, 371–382, 2016.

[6] Abdullah, M. A. H., R. S. M. Rashid, M. Amran, F. Hejazii, N. M. Azreen, R. Fediuk, Y. L. Voo, N. I. Vatin, and M. I. Idris, "Recent trends in advanced radiation shielding concrete for construction of facilities: Materials and properties," *Polymers*, Vol. 14, No. 14, 2830, 2022.

[7] Choppin, G., J.-O. Liljenzin, and J. Rydberg, *Radiochemistry and Nuclear Chemistry: Of Nuclear Chemistry, Theory and Applications*, Elsevier, 2016.

[8] Valković, V., "Radiation safety," *Radioactivity in the Environment*, Vol. 23, 259–303, 2000.

[9] Ogawa, M., Y. Nakajima, R. Kubota, and Y. Endo, "Two cases of acute lead poisoning due to occupational exposure to lead," *Clinical Toxicology*, Vol. 46, No. 4, 332–335, 2008.

[10] Hendrie, J. M., "Nuclear power plants: Structure and function," *Bulletin of the New York Academy of Medicine*, Vol. 59, No. 10, 870, 1983.

[11] Nikbin, I. M., M. Shad, G. A. Jafarzadeh, and S. Dezhampanah, "An experimental investigation on combined effects of nano-WO_3 and nano-Bi_2O_3 on the radiation shielding properties of magnetite concretes," *Progress in Nuclear Energy*, Vol. 117, 103103, 2019.

[12] Nikbin, I. M., S. Mehdipour, S. Dezhampanah, R. Mohammadi, R. Mohebbi, H. H. Moghadam, and A. Sadrmomtazi, "Effect of high temperature on mechanical and gamma ray shielding properties of concrete containing nano-TiO_2," *Radiation Physics and Chemistry*, Vol. 174, 108967, 2020.

[13] Azreen, N. M., R. S. M. Rashid, Y. H. M. Amran, Y. L. Voo, M. Haniza, M. Hairie, R. Alyousef, and H. Alabduljabbar, "Simulation of ultra-high-performance concrete mixed with hematite and barite aggregates using Monte Carlo for dry cask storage," *Construction and Building Materials*, Vol. 263, 120161, 2020.

[14] Janković, K., S. Stanković, D. Bojović, M. Stojanović, and L. Antić, "The influence of nano-silica and barite aggregate on properties of ultra high performance concrete," *Construction and Building Materials*, Vol. 126, 147–156, 2016.

[15] Binici, H., "Durability of heavyweight concrete containing barite," *International Journal of Materials Research*, Vol. 101, No. 8, 1052–1059, 2010.

[16] Oto, B., N. Yıldız, F. Akdemir, and E. Kavaz, "Investigation of gamma radiation shielding properties of various ores," *Progress in Nuclear Energy*, Vol. 85, 391–403, 2015.

[17] Akkurt, I., C. Basyigit, S. Kilincarslan, B. Mavi, and A. Akkurt, "Radiation shielding of concretes containing different aggregates," *Cement and Concrete Composites*, Vol. 28, No. 2, 153–157, 2006.

[18] Shah, A. Z., M. H. M. Zaid, K. A. Matori, Y. Yaakob, A. R. Sarmani, and R. Hisam, "Comprehensive study on structural, elastic and radiation shielding abilities of novel quaternary Bi_2O_3-TeO_2-Li_2O-Al_2O_3 glasses," *Progress in Nuclear Energy*, Vol. 171, 105191, 2024.

[19] Sayyed, M. I., Y. Al-Hadeethi, M. M. AlShammari, M. Ahmed, S. H. Al-Heniti, and Y. S. Rammah, "Physical, optical and gamma radiation shielding competence of newly boro-tellurite based glasses: TeO_2-B_2O_3-ZnO-Li_2O_3-Bi_2O_3," *Ceramics International*, Vol. 47, No. 1, 611–618, 2021.

[20] Rajesh, D., Y. C. Ratnakaram, M. Seshadri, and A. Balakrishna, "Luminescence properties of Sm3+ impurities in strontium lithium bismuth borate glasses," in *AIP Conference Proceedings*, Vol. 1447, No. 1, 581–582, 2012.

[21] Annapoorani, K., C. Basavapoornima, N. S. Murthy, and K. Marimuthu, "Investigations on structural and luminescence behavior of Er3+ doped Lithium Zinc borate glasses for lasers and optical amplifier applications," *Journal of Non-Crystalline Solids*, Vol. 447, 273–282, 2016.

[22] Arora, R., N. Kaur, H. Singh, D. Kumar, V. Bhatia, and S. P. Singh, "B_2O_3-TeO_2-ZnO-Na_2O-Nd_2O_3 glass matrices: A comprehensive study of physical, structural, optical, and thermoluminescence properties," *Materials Chemistry and Physics*, Vol. 313, 128783, 2024.

[23] Laxmikanth, C., A. M. Elias, S. Sichone, and B. Mwankemwa, "Tailoring structural, thermal, and optical properties of Tm3+-doped borotellurite glasses through Bi_2O_3 incorporation for optical fiber construction," *Next Materials*, Vol. 6, 100274, 2025.

[24] Asri, M., M. Ahmadi, and V. Zanganeh, "Study of optical properties and comprehensive shielding behaviors for neutron and gamma-ray of $60Bi_2O_3$-$(40 - x)$ B_2O_3-xBaO glass system," *Results in Physics*, Vol. 52, 106824, 2023.

[25] Yin, S., H. Wang, A. Li, Z. Ma, and Y. He, "Study on radiation shielding properties of new barium-doped zinc tellurite glass," *Materials*, Vol. 15, No. 6, 2117, 2022.

[26] Abdelghany, Y. A., M. M. Kassab, M. M. Radwan, *et al.*, "Investigation of optical, mechanical, and shielding properties of zirconia glass capsule," *Progress in Nuclear Energy*, Vol. 154, 104457, 2022.

[27] Şakar, E., O. F. Özpolat, B. Alım, M. I. Sayyed, and M. Kurudirek, "Phy-X/PSD: Development of a user friendly online software for calculation of parameters relevant to radiation shielding and dosimetry," *Radiation Physics and Chemistry*, Vol. 166, 108496, 2020.

[28] Gökçe, H. S., O. Güngör, and H. Yılmaz, "An online software to simulate the shielding properties of materials for neutrons and photons: NGCal," *Radiation Physics and Chemistry*, Vol. 185, 109519, 2021.

[29] Alhassan, M., S. I. Muazu, and H. A. Ibrahim, "Construction of mathematical equation to predict the densities of BaO-B_2O_3-Bi_2O_3 glass system using the percentage weights of its constituents," *World Journal of Advanced Engineering Technology and Sciences*, Vol. 8, No. 1, 090–096, 2023.

[30] Alshamari, A., M. H. A. Mhareb, N. Alonizan, M. I. Sayyed, N. Dwaikat, I. Alrammah, M. K. Hamad, and Q. A. Drmosh, "Gamma-ray-induced changes in the radiation shielding, structural, mechanical, and optical properties of borate, tellurite, and borotellurite glass systems modified with barium and bismuth oxide," *Optik*, Vol. 281, 170829, 2023.

[31] Al-Shelkamy, S. A., H. R. Vega-Carrillo, Z. Xie, F. M. El-Hossary, E. S. Mosa, A. A. Mahdy, O. Elkady, M. A. Ghafaar, *et al.*, "Mechanical and radiation shielding characterization of W-based alloys for advanced nuclear unit," *Applied Radiation and Isotopes*, Vol. 201, 110995, 2023.

[32] Al-Buriahi, M. S. and B. T. Tonguc, "Mass attenuation coefficients, effective atomic numbers and electron densities of some contrast agents for computed tomography," *Radiation Physics and Chemistry*, Vol. 166, 108507, 2020.

[33] Abdel-Latif, M. A. and Kassab, "Effect of chromium contents on radiation shielding and macroscopic cross-section in steel alloys," *Applied Radiation and Isotopes*, Vol. 186, 110263, 2022.

[34] Monazie, A. M., A. M. A. Kaisy, A. F. Tawfic, S. A. Al-Shelkamy, *et al.*, "Shielding and dosimetry parameters for aluminum carbon steel," *Applied Radiation and Isotopes*, Vol. 201, 111022, 2023.

[35] Al-Buriahi, M. S., F. I. El-Agawany, C. Sriwunkum, H. Akyıldırım, H. Arslan, B. T. Tonguc, R. El-Mallawany, and Y. S. Rammah, "Influence of Bi_2O_3/PbO on nuclear shielding characteristics of lead-zinc-tellurite glasses," *Physica B: Condensed Matter*, Vol. 581, 411946, 2020.

[36] Abdel-Latif, A., M. Kassab, M. I. Sayyed, and H. O. Tekin, "Optimizing the shielding properties of strength-enhanced concrete containing marble," *Papers in Physics*, Vol. 12, 120 005–120 005, 2020.

[37] Tamam, N., M. A. Huwayz, Z. A. Alrowaili, N. Alwadai, K. M. Katubi, M. S. Alqahtani, I. O. Olarinoye, and M. S. Al-Buriahi, "Radiation attenuation of boro-tellurite glasses for efficient shielding applications," *Applied Radiation and Isotopes*, Vol. 203, 111080, 2024.

[38] Rammah, Y. S., K. A. Mahmoud, M. I. Sayyed, F. I. El-Agawany, and R. El-Mallawany, "Novel vanadyl lead-phosphate glasses: P_2O_5-PbO-ZnONa_2O-V_2O_5: Synthesis, optical, physical and gamma photon attenuation properties," *Journal of Non-Crystalline Solids*, Vol. 534, 119944, 2020.

[39] El-Khayatt, A. M., "NXcom-A program for calculating attenuation coefficients of fast neutrons and gamma-rays," *Annals of Nuclear Energy*, Vol. 38, No. 1, 128–132, 2011.

[40] El-Khayatt, A. M. and A. E.-S. Abdo, "MERCSF-N: A program for the calculation of fast neutron removal cross sections in composite shields," *Annals of Nuclear Energy*, Vol. 36, No. 6, 832–836, 2009.

[41] El-Khayatt, A. M., "Calculation of fast neutron removal cross-sections for some compounds and materials," *Annals of Nuclear Energy*, Vol. 37, No. 2, 218–222, 2010.

[42] Elmahroug, Y., B. Tellili, and C. Souga, "Calculation of fast neutron removal cross-sections for different shielding materials," *International Journal of Physics and Research (IJPR)*, Vol. 3,

No. 2, 7–16, 2013.

[43] Kassab, M. M., S. U. El-Kameesy, M. M. Eissa, *et al.*, "A study of neutron and gamma-ray interaction properties with cobalt-free highly chromium maraging steel," *Journal of Modern Physics*, Vol. 6, No. 11, 1526, 2015.

[44] Al-Buriahi, M. S., Y. S. M. Alajerami, A. S. Abouhaswa, A. Alalawi, T. Nutaro, and B. Tonguc, "Effect of chromium oxide on the physical, optical, and radiation shielding properties of lead sodium borate glasses," *Journal of Non-Crystalline Solids*, Vol. 544, 120171, 2020.

[45] Kumar, A., "Gamma ray shielding properties of PbO-Li_2O-B_2O_3 glasses," *Radiation Physics and Chemistry*, Vol. 136, 50–53, 2017.

[46] Halimah, M. K., A. Azuraida, M. Ishak, and L. Hasnimulyati, "Influence of bismuth oxide on gamma radiation shielding properties of boro-tellurite glass," *Journal of Non-Crystalline Solids*, Vol. 512, 140–147, 2019.

[47] Alotaibi, B. M., M. I. Sayyed, A. Kumar, M. Alotiby, A. Sharma, H. A. Al-Yousef, N. A. M. Alsaif, and Y. Al-Hadeethi, "Optical and gamma-ray shielding effectiveness of a newly fabricated P_2O_5–CaO–Na_2O–K_2O–PbO glass system," *Progress in Nuclear Energy*, Vol. 138, 103798, 2021.

[48] Abdelghany, Y. A., M. M. Kassab, M. M. Radwan, and M. A. Abdel-Latif, "Borotellurite glass system doped with ZrO_2, potential use for radiation shielding," *Progress in Nuclear Energy*, Vol. 149, 104256, 2022.

[49] Alyami, W., S. A. El-khateeb, E. M. Alkhybari, L. K. Jambi, and I. E. Saad, "Highly transparent glass of barium-reinforced borotellurite as a protective material from gamma rays," *Optical and Quantum Electronics*, Vol. 56, No. 4, 613, Feb. 2024.

[50] Srinivas, B., A. Bhogi, P. Naresh, M. N. Chary, M. Shareefuddin, Z. A. Alrowaili, Z. M. M. Mahmoud, I. O. Olarinoye, and M. S. Al-Buriahi, "Fabrication, optical and radiation shielding properties of BaO-TeO_2-B_2O_3-Cr_2O_3 glass system," *Optik*, Vol. 258, 168877, 2022.

[51] Alothman, M. A., I. O. Olarinoye, C. Sriwunkum, S. Alomairy, J. S. Alzahrani, and M. S. Al-Buriahi, "Study of the radiation attenuation properties of MgO-Al_2O_3-SiO2-Li_2O-Na_2O glass system," *Journal of the Australian Ceramic Society*, Vol. 58, 267–273, Feb. 2022.

[52] Alothman, M. A., Z. A. Alrowaili, A. M. Al-Baradi, O. Kilicoglu, C. Mutuwong, and M. S. Al-Buriahi, "Elastic properties and radiation shielding ability of ZnO-P_2O_5/B_2O_3 glass system," *Journal of Materials Science: Materials in Electronics*, Vol. 32, No. 14, 19 203–19 217, Jun. 2021.

[53] Boukhris, I., I. Kebaili, M. S. Al-Buriahi, B. Tonguc, M. M. Al-Shammari, and M. I. Sayyed, "Effect of bismuth oxide on the optical features and gamma shielding efficiency of lithium zinc borate glasses," *Ceramics International*, Vol. 46, No. 14, 22 883–22 888, 2020.

[54] Al-Buriahi, M. S., M. I. Sayyed, and Y. Al-Hadeethi, "Role of TeO_2 in radiation shielding characteristics of calcium borotellurite glasses," *Ceramics International*, Vol. 46, No. 9, 13 622–13 629, 2020.